

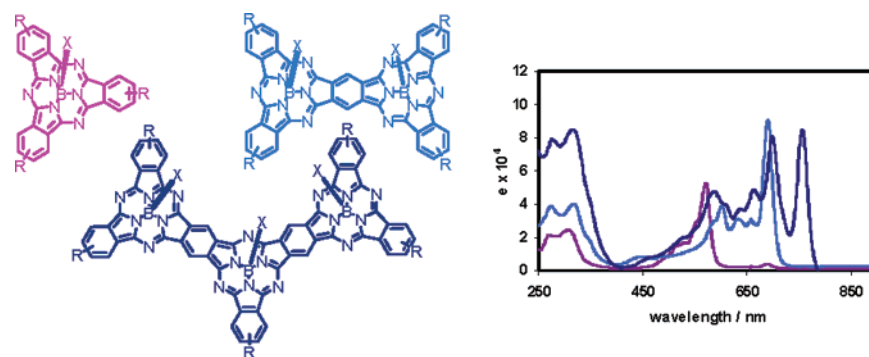
Subphthalocyanine-Fused Dimers and Trimers: Synthetic, Electrochemical, and Theoretical Studies

Rodrigo S. Iglesias,[†] Christian G. Claessens,[†] Tomas Torres,^{*,†} M. Ángeles Herranz,[‡]
Victor R. Ferro,[§] and Jose M. García de la Vega^{*,§}

Departamento de Química Orgánica, Universidad Autónoma de Madrid, 28049-Madrid, Spain,
Departamento de Química Orgánica I, Universidad Complutense de Madrid, 28040-Madrid, Spain, and
Departamento de Química Física Aplicada, Universidad Autónoma de Madrid, 28049-Madrid, Spain

tomas.torres@uam.es

Received December 19, 2006



Subphthalocyanine (SubPc)-fused dimers and trimers bearing fluorine, iodine, and thioether peripheral substituents were synthesized and characterized. Absorption spectroscopy and electrochemical studies revealed (i) that the substituents have a strong effect on the electronic properties of the macrocycles and (ii) that there is good communication between the subphthalocyaninic moieties within the oligomeric structures. Theoretical calculations at DFT/6-31G(d,p) computational level and electron density studies support the experimental findings. The frontier orbitals in the dimers and trimers were also shown to be significantly altered with respect to those of SubPcs as a consequence of the extension of the conjugation associated with symmetry breaking. Time-dependent density functional theory calculations reproduced the differences observed in the UV–vis spectra of the fused dimers and the monomeric SubPcs.

Introduction

Subphthalocyanines¹ (SubPcs, Figure 1) are lower homologues of phthalocyanines, consisting of three diiminoisoindole units *N*-fused around a central boron atom. These cone-shaped

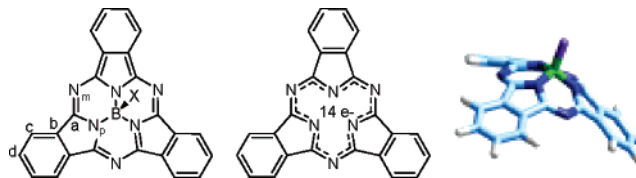


FIGURE 1. SubPc. Structure and electron delocalization.

macrocycles comprise an aromatic 14 π -electron system, which provides interesting electronic properties that allow their application as dyes for technological devices,² as supramolecular building blocks,³ as nonlinear optical chromophores,⁴ and as components in photo- and electroactive dyads and triads.⁵ SubPcs were serendipitously discovered in 1972 by Meller and Ossko as they were trying to synthesize a boron phthalocyanine. Instead, they obtained a magenta compound that was unambiguously characterized by elemental analysis and mass spectrom-

[†] Departamento de Química Orgánica, Universidad Autónoma de Madrid.

[‡] Universidad Complutense de Madrid.

[§] Departamento de Química Física Aplicada, Universidad Autónoma de Madrid.

(1) (a) Torres, T. *Angew. Chem., Int. Ed.* **2006**, *45*, 2834–2837. (b) Claessens, C. G.; González-Rodríguez, D.; Torres, T. *Chem. Rev.* **2002**, *102*, 835–853.

(2) (a) Torres, T.; Claessens, C. G.; Iglesias, R. S.; González-Rodríguez, D.; Martínez-Díaz, M. V. (Universidad Autónoma de Madrid, Spain.) Spanish Patent ES 200401615, 2005. (b) Yanagimoto, T.; Yamada, H.; Tsuchiya, M.; Kawasato, H. (Nippon Steel Chemical Co., Ltd., Japan) WO 2004067644, 2004, *Chem. Abstr.* **2004**, *141*, 191923. (c) Zafirov, A.; Rakovski, S.; Bakardjieva-Eneva, J.; Prahov, L.; Assenova, L.; Marrandino, F. (Vivastar Mastering & Materials A.-G., Switz.) WO 2002080158, 2002, *Chem. Abstr.* **2002**, *137*, 318007.

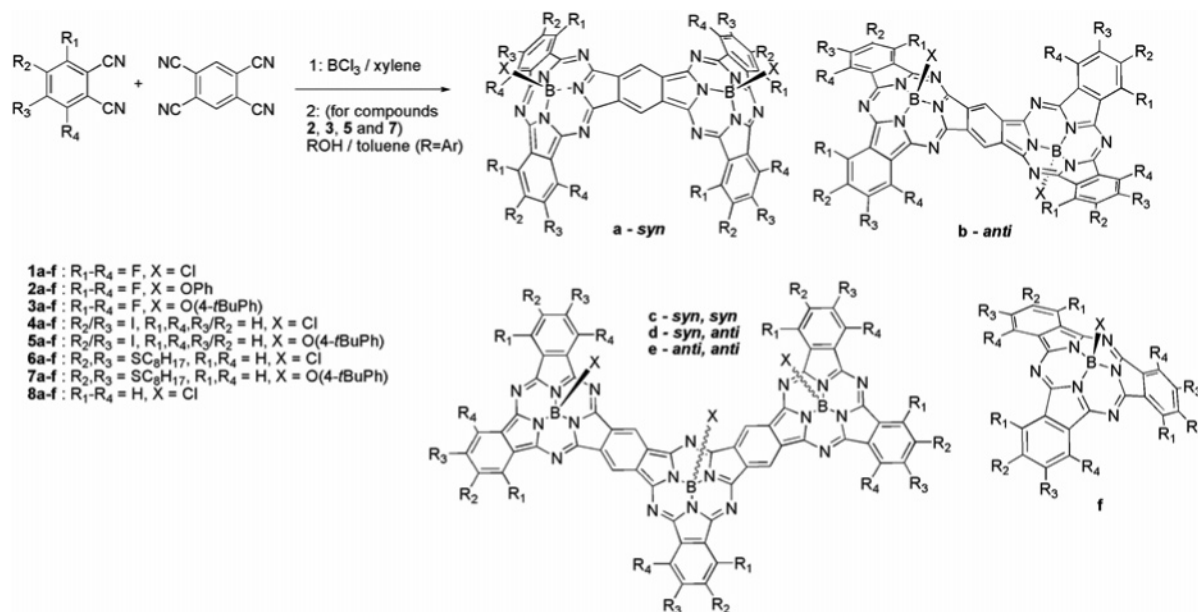


FIGURE 2. Structure of SubPc Dimers (a, b), Trimers (c, d, e), and monomeric SubPc (f) with different peripheral and axial substituents (1–8).

etry. Two years later, an X-ray crystal structure further confirmed the former structural claims.

One of our current research interests is focused on the development of extended π -surfaces using phthalocyanines and homologous macrocycles as building blocks.⁶ Large conjugated molecules may present several interesting properties, as the electronic absorption in the visible region (Q-band) is shifted to the infrared or near-infrared spectral regions (higher than ~ 700 nm), which can be explored in many applications such as electrolithography (printing technologies), sensitization for photovoltaic devices, or photodynamic therapies.⁷ Also, extended π -electronic surfaces are highly polarizable, which is a

desired feature for a molecule to present third-order nonlinear optical behavior, and consequently may be employed in nonlinear optical applications.⁸

Recently, significant amelioration⁹ of the SubPc formation reaction led us and others to the elaboration of more complex structures such as fused SubPc dimers and trimers (Figure 2), hereafter referred to as Dimers and Trimers.¹⁰

A similar Dimer was first mentioned in a preliminary communication by Kobayashi et al. even if, at that time, the author failed to fully characterize it.¹¹ As a matter of fact, these fused systems possess the added interest that they are among the very few known examples of curved π -surfaces.¹²

Unlike most of the fused phthalocyanine¹³ and porphyrazine¹⁴ dimers, which present very similar UV–vis absorption features with respect to the corresponding mononuclear macrocycles,

(3) (a) Claessens, C. G.; Torres, T. *Chem. Commun.* **2004**, 11, 1298–1299. (b) Berner, S.; De Wild, M.; Ramoino, L.; Ivan, S.; Barattoff, A.; Guentherodt, H.-J.; Suzuki, H.; Schlettwein, D.; Jung, T. A. *Phys. Rev. B* **2003**, 68, 115410/1–115410/11. (c) Claessens, C. G.; Torres, T. *J. Am. Chem. Soc.* **2002**, 124, 14522–14523. (d) De Wild, M.; Berner, S.; Suzuki, H.; Yanagi, H.; Schlettwein, D.; Ivan, S.; Barattoff, A.; Guentherodt, H.-J.; Jung, T. A. *Chem. Phys. Chem.* **2002**, 3, 881–885.

(4) (a) Claessens, C. G.; de la Torre, G.; Torres, T. In *Nonlinear Optical Properties of Matter: From Molecules to Condensed Phases*; Papadopoulos, M.G., Sadlej, A.J., Leszczynski, J., Eds.; Springer, Dordrecht, The Netherlands, 2006; Vol. 1, pp 509–535. (b) Claessens, C. G.; González-Rodríguez, D.; Torres, T.; Martín, G.; Agulló-López, F.; Ledoux, I.; Zyss, J.; Ferro, V. R.; de la Vega, J. M. *J. Phys. Chem. B* **2005**, 109, 3800–3806. (c) Martín, G.; Rojo, G.; Agulló-López, F.; Ferro, V. R.; García de la Vega, J. M.; Martínez-Díaz, M. V.; Torres, T.; Ledoux, I.; Zyss, J. *J. Phys. Chem. B* **2002**, 106, 13139–13145. (d) del Rey, B.; Keller, U.; Torres, T.; Rojo, G.; Agulló-López, F.; Nonell, S.; Marti, C.; Brasselet, S.; Ledoux, I.; Zyss, J. *J. Am. Chem. Soc.* **1998**, 120, 12808–12817.

(5) (a) González-Rodríguez, D.; Claessens, C. G.; Torres, T.; Liu, S.-G.; Echegoyen, L.; Vila, N.; Nonell, S. *Chem.–Eur. J.* **2005**, 15, 3881–3893. (b) Iglesias, R. S.; Claessens, C. G.; Torres, T.; Aminur Arman, G. M.; Guldi, D. M. *Chem. Commun.* **2005**, 2113–2115. (c) González-Rodríguez, D.; Torres, T.; Guldi, D. M.; Rivera, J.; Herranz, M. A.; Echegoyen, L. *J. Am. Chem. Soc.* **2004**, 126, 6301–6313. (d) González-Rodríguez, D.; Torres, T.; Guldi, D. M.; Rivera, J.; Echegoyen, L. *Org. Lett.* **2002**, 4, 335–338.

(6) (a) García-Frutos, E. M.; Fernández-Lazaro, F.; Maya, E. M.; Vázquez, P.; Torres, T. *J. Org. Chem.* **2000**, 65, 6841–6846. (b) de la Torre, G.; Martínez-Díaz, V.; Ashton, P. R.; Torres, T. *J. Org. Chem.* **1998**, 63, 8888–8893. (c) Maya, E. M.; Vázquez, P.; Torres, T. *Chem.–Eur. J.* **1999**, 5, 2004–2013.

(7) (a) Fabian, J.; Nakazumi, H.; Matsuoaka, N. *Chem. Rev.* **1992**, 92, 1197–1226. (b) Perepichka, D. F.; Bryce, M. R. *Angew. Chem., Int. Ed.* **2005**, 44, 5370–5373.

(8) (a) Zyss, J.; Ledoux, I. *Chem. Rev.* **1994**, 94, 77–105. (b) de la Torre, G.; Torres, T.; Vázquez, P.; Agulló-López, F. *Chem. Rev.* **2004**, 104, 3723–3750.

(9) (a) Claessens, C. G.; Torres, T. *Chem.–Eur. J.* **2000**, 6, 2168–2172. (b) Claessens, C. G.; Torres, T. *Tetrahedron Lett.* **2000**, 41, 6361–6365. (c) Claessens, C. G.; González-Rodríguez, D.; del Rey, B.; Torres, T.; Mark, G.; Schuchmann, H.-P.; von Sonntag, C.; MacDonald, G.; Nohr, R. S. *Eur. J. Org. Chem.* **2003**, 2547–2551.

(10) (a) Claessens, C. G.; Torres, T. *Angew. Chem., Int. Ed.* **2002**, 41, 2561–2565. (b) Fukuda, T.; Stork, J. R.; Potucek, R. J.; Olmstead, M. M.; Noll, B. C.; Kobayashi, N.; Durfee, W. S. *Angew. Chem., Int. Ed.* **2002**, 41, 2565–2568.

(11) Kobayashi, N. *Chem. Commun.* **1991**, 1203–1204.

(12) (a) Yamaguchi, Y. *J. Chem. Phys.* **2004**, 120, 7963–7970. (b) Kawase, T.; Tanaka, K.; Shiono, N.; Seirai, Y.; Oda, M. *Angew. Chem., Int. Ed.* **2004**, 43, 1722–1724. (c) Scott, L. T. *Angew. Chem., Int. Ed.* **2003**, 42, 4133–4135. (d) Reiher, M.; Hirsch, A. *Chem.–Eur. J.* **2003**, 9, 5442–5452.

(13) (a) Makarov, S.; Litwinski, C.; Ermilov, E. A.; Suvorova, O.; Roeder, B.; Wöhrle, D. *Chem.–Eur. J.* **2006**, 12, 1468–1474. (b) Zhang, Q. M.; Li, H.; Poh, M.; Xia, F.; Cheng, Z.-Y.; Xu, H.; Huang, C. *Nature* **2002**, 419, 284–287. (c) Liu, C.; Wang, X.; Gong, Q.; Liu, Y.; Qiu, W.; Zhu, D. *Chem. Phys. Lett.* **2001**, 347, 378–382. (d) Kobayashi, N.; Fukuda, T.; Lelièvre, D. *Inorg. Chem.* **2000**, 39, 3632–3637. (e) Ishii, K.; Kobayashi, N.; Higashi, Y.; Osa, T.; Lelièvre, D.; Simon, J.; Yamauchi, S. *Chem. Commun.* **1999**, 969–970. (f) Zhang, Y. J.; Li, L. S.; Jin, J.; Jiang, S.; Zhao, Y.; Li, T. J.; Du, X.; Yang, S. *Langmuir* **1999**, 15, 2183–2187. (g) Kobayashi, N.; Lam, H.; Nevin, W. A.; Janda, P.; Leznoff, C. C.; Koyama, T.; Monden, A.; Shirai, H. *J. Am. Chem. Soc.* **1994**, 116, 879–90.

TABLE 1. Yields of SubPc **1f** and Dimer (**1a**+**1b**) Obtained at Various Tetrafluorophthalonitrile/Tetracyanobenzene Ratios

entry	tetrafluorophthalonitrile/ tetracyanobenzene ratio	yield (%)	
		dimers ^a	SubPc
1	1:2	<1	26
2	1:1	3	32
3	5:1	5	40
4	10:1	20	43
5	20:1	16	58

^a Yields correspond to the sum of the *anti* and *syn* topoisomers.

the Dimers and Trimers were shown to display a huge bathochromic shift of their Q-band (120 and 180 nm, respectively) when compared to the corresponding monomeric SubPc, thus conferring them a distinctive blue color in solution. Furthermore, the Q-bands of both Dimers and Trimers have a very typical multiband fine structure comprising four major absorptions, a fact that has not received any explanation so far.

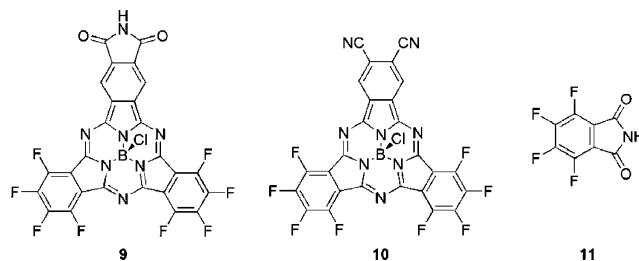
In this article we will describe (i) a brief study of the influence on the outcome of the reaction of some of the most important reaction parameters involved in the preparation of the Dimers and Trimers so as to optimize their yield of formation and (ii) the subsequent synthesis of new Dimers and Trimers bearing different peripheral and axial substituents. Furthermore, through theoretical calculations, we will give a tentative explanation for the relative stability, the electrochemical behavior, and the UV–vis absorption data of these singular aromatic compounds.

Results and Discussion

Synthesis. The condensation reaction between tetrafluorophthalonitrile and 1,2,4,5-tetracyanobenzene in the presence of boron trichloride that led to Dimers **1a–b** and Trimers **1c–e** was studied more thoroughly in order to determine the optimal reaction conditions. The choice of tetrafluorophthalonitrile relied on the following assumptions: (i) it provides solubility to the macrocycle, (ii) its symmetry allows an easier NMR characterization, and (iii) it is stable under the SubPc formation reaction conditions. Furthermore, topoisomers **1a** and **1b** can be easily purified by column chromatography on silica gel and characterized individually.

The synthesis was performed with five different tetrafluorophthalonitrile/tetracyanobenzene ratios (Table 1), leaving all the other reaction parameters unchanged. The three ratios involving higher quantities of tetracyanobenzene (entries 1–3) resulted in very poor yields of Dimers (less than 5%), probably as a consequence of the formation of insoluble tetracyanobenzene polycondensation products. When the ratio is greater than 10:1 (entries 4–5), reasonable yields of Dimers (around 20%) were obtained. In order to minimize the formation of dodecafluorophthalocyanine **1f** a 10:1 phthalonitrile/tetracyanobenzene ratio was used in all subsequent reactions.

The condensation reaction was carried out at temperatures ranging from 80 °C to reflux temperature of *p*-xylene (138 °C), and the best yield was obtained at reflux, which is also the optimal temperature for the synthesis of SubPcs under similar conditions.⁹

**FIGURE 3.** Octafluorophthalimide SubPc **9**, dicyano-octafluoro SubPc **10**, and tetrafluorophthalimide **11**.

The axial functionalization of Dimers **1a–b** was achieved by refluxing the crude product from the condensation reaction between tetrafluorophthalonitrile, tetracyanobenzene and boron trichloride with phenol or 4-*tert*-butylphenol in toluene for 16–24 h. In this way, axially functionalized Dimers **2a–b** and **3a–b** were obtained in 13 and 19% yields, respectively. Reaction of pure **1a–b** with the corresponding phenol derivatives in toluene at reflux led to **2a–b** and **3a–b** in 11 and 17% overall yields from starting tetracyanobenzene.

Other relevant compounds were identified in the course of the purification procedures (Figure 3). Thus for example, an asymmetric octafluoro-phthalimido SubPc **9** was isolated in 16% yield when a 2:1 tetrafluorophthalonitrile/tetracyanobenzene ratio was employed (Table 1, entry 1) and fully characterized. This compound helps to give a deeper insight into the mechanism of SubPc formation since it can only result from the hydrolysis of a more reactive intermediate that most probably comes from the reaction between a dicyanoSubPc **10** and boron trichloride. Tetrafluorophthalimide¹⁵ **11** could also be isolated from this reaction in 12% yield.

Dimers **4a–b** could not be isolated from the condensation reaction between 4-iodophthalonitrile and tetracyanobenzene in the presence of boron trichloride as a consequence of their low solubility. Instead, Dimers **5a–b** were obtained in a one-pot procedure by reacting the crude from the condensation reaction between 4-iodophthalonitrile, tetracyanobenzene, and BCl₃ with 4-*tert*-butylphenol in toluene at reflux. Compounds **5a,b** can potentially exist as 14 different isomers (7 *syn* and 7 *anti*), six of them being chiral structures (Figure 4). Even if the isolation of each possible isomer could not be achieved, two groups of *syn* isomers and one of *anti* were isolated, in very low yields (less than 1% for each group), by column chromatography on silica gel.

Dimers **6a–b** could not be isolated as a consequence of their quick decomposition on silica gel. Instead, octaethylthioether-substituted Dimers **7a,b** were obtained in 16% yield (**7a**, 9%; **7b**, 7%) from the condensation of 3,4-diethylthiophthalonitrile and 1,2,4,5-tetracyanobenzene in the presence of boron trichloride in *p*-xylene followed by axial substitution with 4-*tert*-butylphenol following the above-mentioned procedure. Their purification was somewhat tedious as a consequence of their tendency to form aggregates in polar solvents as it may be anticipated from the presence of eight long alkyl chains. The corresponding Trimers **7c–e** could also be isolated and characterized as a mixture of the three possible topoisomers in 0.2% yield.

Characterization. All compounds were characterized by ¹H NMR, high-resolution mass spectrometry, elemental analysis, and UV–vis spectrophotometry among other techniques.

(14) (a) Luo, Q.; Cheng, S.; Tian, H. *Tetrahedron Lett.* **2004**, *45*, 7737–7740. (b) Garrido Montalban, A.; Jarell, W.; Riguet, E.; McCubbin, Q. J.; Anderson, M. E.; White, A. J. P.; Williams, D. J.; Barrett, A. G. M.; Hoffman, B. M. *J. Org. Chem.* **2000**, *65*, 2472–2478.

(15) Gething, B.; Patrick, C. R.; Tatlow, J. C. *J. Chem. Soc. Abstr.* **1961**, 1574–1576.

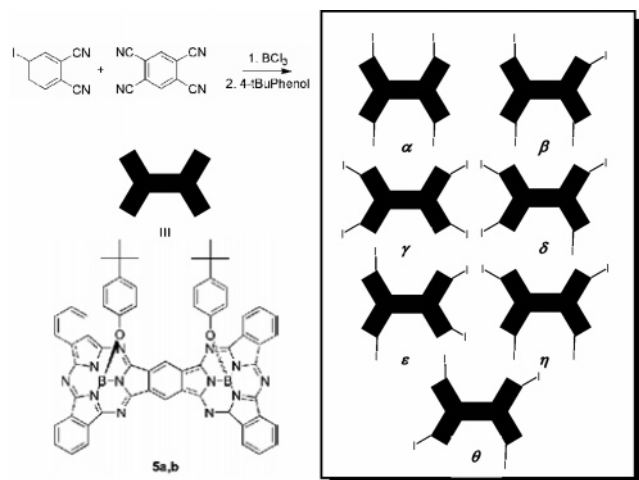


FIGURE 4. Possible isomers of the iodo-substituted Dimers: isomers **5a**, **5b**, **5c**, **5d**, **5e**, **5f**, **5g**, and **5h** are chiral structures.

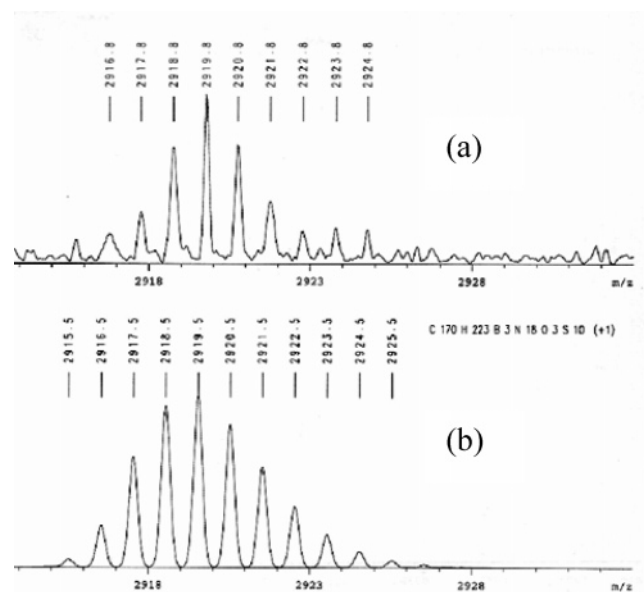
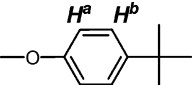


FIGURE 5. Experimental (a) and theoretical (b) isotopic pattern for the $[M]^+$ ion of Trimers **7c–e** as determined by matrix-assisted laser desorption–ionization time-of-flight (MALDI-TOF) mass spectrometry.

Mass Spectrometry. In all cases, peaks corresponding to the molecular ions of all new species were observed. Moreover, peaks corresponding to the loss of one, two, or three axial substituents, in accordance with the compound, could also be observed. As could be expected, the presence of more than one axial substituent increases the relative proportion of $[M - n(\text{axial substituents})]^+$ with respects to $[M]^+$. The experimental isotopic pattern for $[M]^+$ was found to be in accordance with the theoretical one in all cases as illustrated in the case of Trimers **7c–e** in Figure 5.

^1H NMR. The phenol groups in axial position not only provide increased solubility and stability to SubPcs and Dimers¹⁰ but also in the case of the Dimers the possibility to assign the *syn* and *anti* topologies by means of ^1H NMR^{10a} spectroscopy (see characterization below). ^1H NMR spectra of the Dimers exhibit as a “fingerprint” a singlet around 10.2–10.5 ppm, corresponding to the two highly deshielded protons of the central benzene ring. This deshielding is undoubtedly a consequence of the high diatropic magnetic currents on the central benzene

TABLE 2. Chemical Shifts of the Phenoxy Axial Groups of Dimers **3a–b**, **5a–b**, and **7a–b** and Corresponding SubPcs **3f**, **5f**, and **7f**

SubPc / SubPcDimer		
	H^a	H^b
3a	5.25/5.28	6.71/6.73
3b	5.39/5.42	6.86/6.89
3f	5.25/5.28	6.78/6.81
5a	5.22/5.28	6.65/6.71
5b	5.41/5.48	6.83/6.90
5f	5.23/5.29	6.72/6.78
7a	5.28/5.34	6.66/6.72
7b	5.41/5.47	6.81/6.87
7f	5.30/5.36	6.74/6.80

ring. Even if the magnetic environment of these protons is identical in the case of *syn* and *anti* topologies, it is quite sensitive to the nature of peripheral substituents (10.40 ppm for **2a** and 10.29 ppm for **7a**).

The signals corresponding to axial phenol protons appear at $\delta = 5.2$ – 5.5 and 6.7 – 6.9 ppm in all Dimers (**2a–b**, **3a–b**, **5a–b**, and **7a–b**) and Trimers (**1c–e** and **7c–e**). Signals at 5.2 – 5.5 ppm that correspond to the protons that are closer to the π -surface of the SubPc moiety were employed as probes for the assignment of each topoisoer.^{10a} While in the *anti* isomer the chemical shifts of the aromatic phenolic protons are very similar to those of the corresponding SubPc, in the *syn* isomer the proximity of the axial groups (less than 3 Å) and their resulting interaction shifts significantly the signals with respect to those of the SubPc (ca. 0.2 ppm, Table 2).

UV–Vis. The UV–visible spectra of the Dimers exhibit, as phthalocyanines and related compounds do, a B or Soret band at ca. 320 nm and a Q band in the visible region at ca. 560 nm. Compared to the SubPcs, the Q band of the Dimers is highly red-shifted, by ca. 120 nm (Figure 6).

This is a strong indication that in the Dimers the π -electron conjugation is more extended than in the SubPcs, involving the central benzene ring as observed in electron density calculations (see below). Furthermore, the Q band of the Dimers has a very characteristic shape, presenting always four well-defined bands, possibly due to the lower symmetry, resulting in less orbital degeneration, compared to that of the SubPcs.

It can be noticed that the axial substitution of the Dimers causes only a very small blue-shift, an effect which is also observed in the SubPcs. In SubPcs, it was observed (and supported by theoretical study) that this hypsochromic shift is dependent on the atom directly linked to the boron atom, increasing in the order $\text{O} > \text{Cl} > \text{Br}$.^{16,17} On the other hand, the peripheral substitution has a very strong effect – the absorption of compounds substituted with donor group octylthioether is red-shifted by around 40 nm with respect to the (acceptor) fluoro-substituted compounds. The same behavior was observed in the case of SubPcs.¹⁷ The iodo-substituted Dimers **5a–b** absorb around 700 nm, a small red-shift compared to the

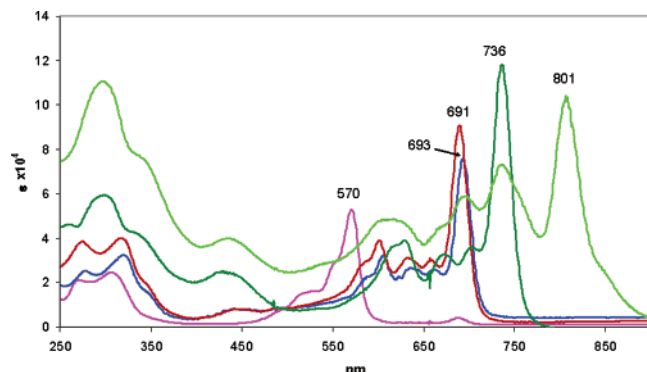
(16) González-Rodríguez, D. Ph.D. Thesis, Universidad Autónoma de Madrid, 2003.

(17) (a) Ferro, V. R.; García de la Vega, J. M.; Claessens, C. G.; Poveda, L. A.; González-Jonte, R. H. *J. Porphyrins Phthalocyanines* **2001**, 5, 491–499. (b) Ferro, V. R.; Poveda, L. A.; Claessens, C. G.; González-Jonte, R. H.; García de la Vega, J. M. *Int. J. Quantum Chem.* **2003**, 91, 369–375.

TABLE 3. Redox Potentials Obtained from Cyclic Voltammetry for the Binuclear SubPc Dimers **1a–b**, **3a–b**, and **7a–b** and Reference SubPcs **1f**, **3f**, and **7f** (THF, in mV vs Fc/Fc⁺)

compound	E^1_{ox} ^a	E^2_{ox} ^a	$E^1_{1/2, red}$	$E^2_{1/2, red}$	compound	E^1_{ox} ^a	E^2_{ox} ^a	$E^1_{1/2, red}$	$E^2_{1/2, red}$	$E^3_{1/2, red}$	$E^4_{1/2, red}$
1f	+1001		−923	−1614 ^b	1b (<i>anti</i>)	+907	+1041	−836	−1130	−1685 ^b	−1918 ^b
					1a (<i>syn</i>)	+870	+1060	−820	−1129	−1551 ^b	−1773 ^b
3f	+989		−1001	−1648	3b (<i>anti</i>)	+865		−928	−1232	−1645	−1857
					3a (<i>syn</i>)	+840		−915	−1213	−1676	−1870
7f	+620	+1000	−1493	−2006 ^b	7b (<i>anti</i>)	+526	+820	−1285	−1585	−2119 ^b	−2346 ^b
					7a (<i>syn</i>)	+500	+798	−1250	−1515	−1964 ^b	−2209 ^b

^a Since these oxidative processes are irreversible, only anodic peak potentials are reported. ^b Since these reductive processes are irreversible, only cathodic peak potentials are given.

**FIGURE 6.** UV-vis spectra of compounds **1f** (purple line), **1b** (red line), **3b** (blue line), **7b** (dark green line), and **7c–e** (light green line).

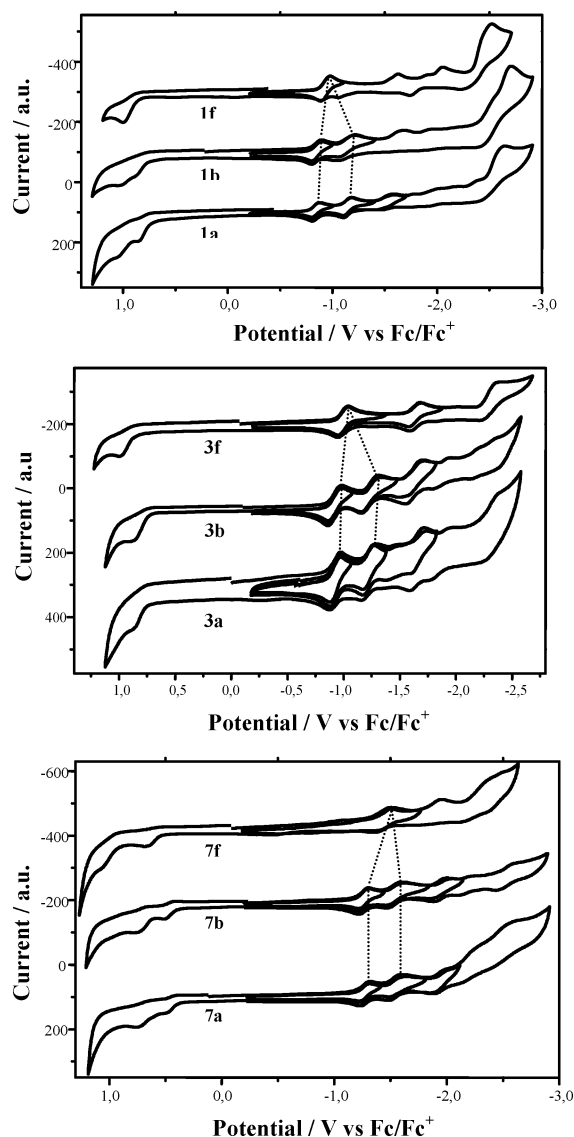
fluoro-substituted ones **2a–b** and **3a–b**. This is due to the lower acceptor effect of iodine compared to that of fluorine.

Also, as expected, the Dimers have a higher molar extinction coefficient than SubPcs (log ϵ around 4.9 in the Dimers and 4.5 in SubPcs), since they possess a larger molecular surface, absorbing more light per molar units.

Electrochemistry. The electrochemical behavior of SubPcs **1f**, **3f**, and **7f** and Dimers **1a–b**, **3a–b**, and **7a–b** was investigated by cyclic voltammetry in THF as summarized in Table 3 and Figure 7. The three SubPcs studied (**1f**, **3f**, and **7f**) exhibit several reduction peaks, with an always reversible first reductive process that involves one electron. At more negative potentials several processes are observed, being the reversibility of them dependent upon the substitution on the macrocycle. In the oxidative part, an irreversible wave is generally observed between 620 and 1001 mV that seems to involve one electron.

Similarly to the electrochemical properties reported for other SubPcs^{5c} a more difficult reduction and an easier oxidation were observed with the increasing donor ability of the substituents in the axial position (chlorine in **1f** vs *tert*-butylphenol in **3f**). In addition, the peripheral substituents on the macrocycle modify strongly the reduction and oxidation potentials of the SubPcs. The SC₈H₁₇ derivative **7f** is much easier to oxidize ($E^1_{ox} = +620$ mV) than the SubPcs bearing fluorine substituents **1f** and **3f** ($E^1_{ox} = +1001$ and $+989$ mV, respectively). The reduction potentials follow the same trend, the first reduction process for **7f** is more than 500 mV cathodically shifted, in comparison with its fluorine-containing analogs **1f** and **3f**.

The π -extended electronic structure of binuclear SubPc dimers strongly impacts the ground state features and, consequently, the electrochemical properties of these structures with respect to those of their corresponding SubPcs (see Table and Figure). The electronic communication between the two SubPc units is clearly appreciated from the variations observed in the redox potentials of the Dimers and reference SubPcs. These observa-

**FIGURE 7.** Cyclic voltammograms of Dimers **1a–b**, **3a–b**, and **7a–b** and the corresponding reference SubPcs **1f**, **3f**, and **7f**.

tions strongly endorse the complete conjugation of the π -electron system in the SubPc Dimers, as previously anticipated.¹⁰

SubPc Dimers exhibit a first oxidation process 100–150 mV negatively shifted when compared to those of the corresponding SubPcs. The second oxidation process, which takes place in the other SubPc subunit, appears up to 300 mV positively shifted when compared to the first one.

In the cathodic scan, the three series of SubPc Dimers exhibit several reduction peaks, with the first two always being

TABLE 4. Root-Mean-square Deviation from the Calculated to Experimental (X-ray Crystallography¹⁰) Bond Distances for Compounds **1a** and **1b**

bond type	B3LYP/6-31G(d,p) (Å)
CC (benzene)	0.015
CC (pyrrole)	0.006
C _a –N _m	0.001
C _a –N _p	0.002
B–N	0.008
B–Cl	0.013
total	0.013

TABLE 5. Calculated Total Electronic Energies (E) and Heat of Formation (ΔH_f) of Some Representative Dimers and SubPcs

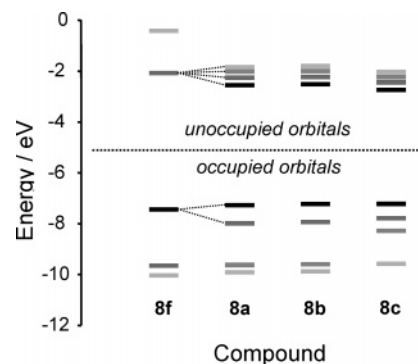
compound	E (au) ^a	ΔH_f^b (kcal/mol)
1a	–4826.3177940	–263.2
1b	–4826.3179259	–263.8
1f	–2926.1765430	–286.6
2a	^c	–234.6
4a	^c	466.7
6a	^c	389.6
8a	–3238.7542665	397.3
8b	–3238.7544775	396.4
8c	–4742.0045783	584.2
8f	–1735.5344175	209.0

^a B3LYP/6-31G(d,p) calculation. ^b AM1 calculation on the B3LYP/6-31G(d,p) optimized geometries. ^c Optimized geometries using semiempirical AM1 method.

reversible and corresponding to the first redox processes on each one of the SubPc subunits. At more negative potentials several processes (up to 7 for **1a**) were observed, being the reversibility of them slightly influenced by the substitution on the macrocycle. The strong coupling existing between both SubPc subunits is also evidenced by the 100–250 mV positive shift that the first reduction potentials experiment when compared with the corresponding SubPc. The second reduction process, which takes place in the other SubPc subunit, appears up to 300 mV negatively shifted when compared with the first one.

Finally, it is important to mention that the electronic communication observed between both SubPc subunits in these Dimers is slightly stronger in the case of the *syn* vs the *anti* isomers. Oxidation potentials appear around 30 mV positively shifted for the *anti* isomers and the same behavior is observed on the reduction potentials, being up to 30 mV negatively shifted in the case of the *anti* isomers when compared with the *syn*.

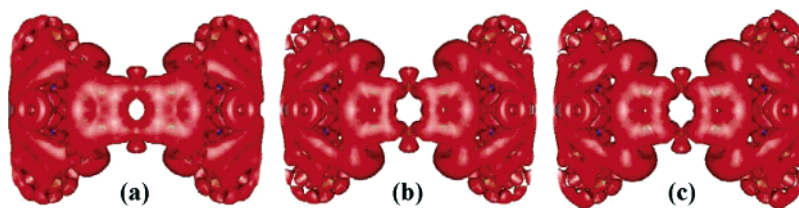
Theoretical Calculations. Geometry. As expected, the DFT-optimized structures employing the B3LYP/6-31G(d,p) method correlate well with the X-ray crystal structures of Dimers **1a** and **1b** as shown by the relatively small root-mean-square deviations from the calculated bond distances to the experimental ones (Table 4). The main discrepancies between experimental and calculated data lies in the overestimation of

**FIGURE 9.** Frontier orbital energies (eV) of Dimers **8a,b**, Trimer **8c**, and reference SubPc **8f** calculated at the B3LYP/6-31G(d,p) computational level.

both B–Cl and C–C (in the benzene groups) bond distances with the B3LYP/6-31G(d,p) method. Geometry optimization employing the semiempirical AM1 parametrization yielded poor results, even if qualitatively reliable, as the minimized structures did not retain the expected (for the *syn* isomer) C_{2v} symmetry.

Energy. Table 5 shows the total electronic energies calculated at the B3LYP/6-31G(d,p) computational level as well as the heat of formation, calculated with the AM1 method on the B3LYP/6-31G(d,p)-optimized geometries, of SubPcs **1f** and **8f**, a representative selection of Dimers and one Trimer. Despite the large size of the structures, calculated energies and heat of formation reproduce well the expected behavior for size increase (SubPc units added) and substituent effects, in a similar way as reported in theoretical studies on SubPcs.¹⁷ The energy difference between *syn* (**1a** and **8a**) and *anti* (**1b** and **8b**) topoisomers is negligible (≤ 1 kcal/mol) suggesting that they do not differ in stability. In contrast, the nature and numbers of substituents in the periphery strongly affect the heat of formation thus, for example, its absolute values for some selected derivatives follow the order: ΔH_f (**1a**) < ΔH_f (**6a**) \approx ΔH_f (**8a**) < ΔH_f (**4a**). In fact, experimentally, it was corroborated that Dimer **1a** is much more stable than Dimers **4a**, **6a**, and **8a** both in solution and in the solid state. Axial substitution was shown to affect the stability of the overall structure (ΔH_f (**1a**) < ΔH_f (**2a**)), most probably as simple consequence of the increase in size by addition of phenoxy groups. The orientation of the phenoxy axial groups in Dimer **2a** has only minor effects on ΔH_f . Conformations with both phenyl groups pointing away from each other are more stable than those with the groups in proximity, by ca. 2 kcal/mol. The same trend is observed in the *anti* topoisomers **2b**, indicating that differences in ΔH_f are not related to interactions between the axial groups.

Electron Density Distribution. Figure 8 shows the contour surfaces of the electron density deformations for the *syn* Dimer

**FIGURE 8.** Contour surface of the electron density deformation for the *syn* SubPc Dimer (a) and its single (b) and double (c) negatively charged derivatives. (Only the charge accumulation is represented. Contour value = 0.001 au. The electron density was calculated at B3LYP/6-31G(d,p) level. The electron density profiles obtained for singly and double charged cations are similar to those of the single and double anions.)

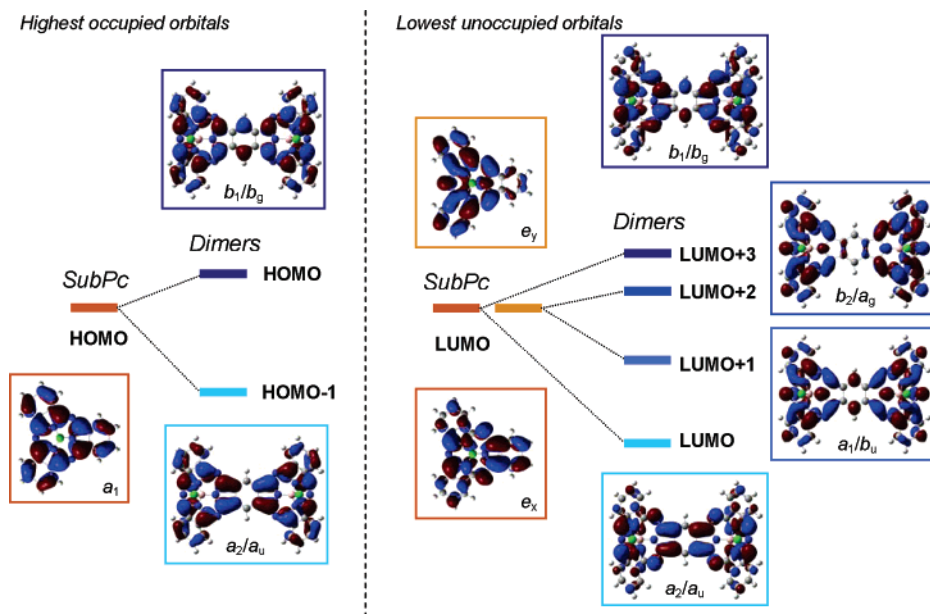


FIGURE 10. Frontier orbitals (highest occupied and lowest unoccupied) of Dimer **8a** and SubPc **8f** calculated at the B3LYP/6-31G(d,p) computational level.

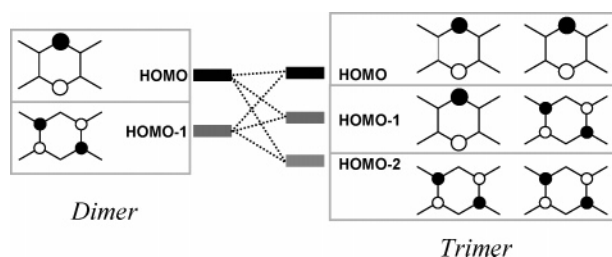


FIGURE 11. Central benzene highest occupied molecular orbitals of Dimer **8a** and Trimer **8c**.

8a and its single and double anions. The neutral *syn* Dimer (**a**) shows a strong π -conjugation in the central part of the molecule involving the condensed benzene ring and the two neighboring pyrrole units. This π electron cloud is connected to the π clouds of the SubPc monomers throughout the electron lone pairs of the meso nitrogens.

Adding/extracting one or two electrons to/from the Dimer partially breaks its π -conjugation. The π -electron cloud of the fused benzene is broken, and as can be expected, the conjugation of the pyrrole units within the individual SubPc moieties is reinforced with a greater meso nitrogens participation.

Molecular Orbitals. Orbital energies of some representative SubPc Dimers (**8a–b**), a SubPcTrimer (**8c**), and a reference SubPc (**8f**) are represented in Figure 9. It is clearly noticed that there are no substantial differences between the frontier orbitals belonging to the *anti* and *syn* isomers **8a** and **8b**, as would be expected considering their nearly identical UV–vis spectra. The most important feature is the breaking of the C_{3v} symmetry of the SubPcs brought about by condensation of the macrocycles, which causes many of its orbitals to split in the fused compounds. The HOMO orbital, for example, is divided in a more unstable b_1 (or b_g for *anti* isomer) orbital and a stabilized a_2 (a_u for the *anti*) orbital in the Dimers, corresponding to the highest-occupied molecular orbital (HOMO) and HOMO-1, respectively.

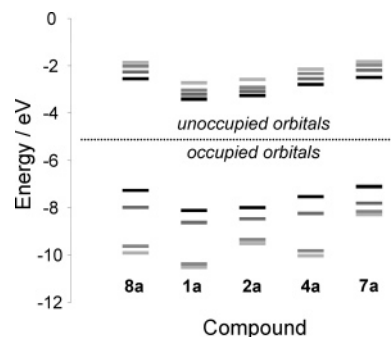


FIGURE 12. Effect of substituents on frontier orbitals of some SubPc Dimers.

These orbitals are combinations of the SubPc HOMO orbital, being similar in shape, with differences contributions in the central benzene (Figure 10).

The HOMO and HOMO-1 orbitals of the Dimers are further split into three orbitals when a third SubPc unit is added (Trimers), now as a consequence of a linear combination of the central benzene different contributions in the HOMO and HOMO-1 of the fused dimers (Figure 11).

The lowest-unoccupied molecular orbital (LUMO) of SubPcs are doubly degenerate (e_x and e_y) as a consequence of the C_3 symmetry of the structure.¹⁸ This degeneracy is broken, and the orbitals are split in the SubPc fused compounds, giving rise to four orbitals very close in energy. The e_x SubPc orbitals becomes an a_2 (or a_u for the *anti* topoisomer) (LUMO) and a b_1 (or b_g) (LUMO+3) in the SubPcDimers, while the e_y becomes a_1/b_u (LUMO+1) and b_2/a_g (LUMO+2) orbitals (Figure 10).

It is interesting to notice that no significant destabilization of the HOMO orbital is detected with increasing number of SubPc units. On the contrary, the LUMO orbitals are substantially *stabilized* with each added SubPc (Figure 9). This not

(18) Kobayashi, N.; Ishizaki, T.; Ishii, K.; Konami, H. *J. Am. Chem. Soc.* **1999**, *121*, 9096–9110.

TABLE 6. Calculated (TDDFT) and Experimental Electronic Transitions of SubPcDimer 1a

electronic transition ^a	oscillator strength	transition wavelength(eV)	
		calcd	exptl
HOMO → LUMO (0.64) ^b	0.97	2.02	1.80
HOMO → LUMO+1 (0.66)	0.25	2.17	1.89
HOMO-1 → LUMO (0.64)	0.02	2.47	1.93
HOMO → LUMO+3 (0.28)			
HOMO-1 → LUMO (0.17)	0.05	2.73	
HOMO → LUMO+3 (0.60)			
HOMO-1 → LUMO+2 (0.67)	0.33	2.82	2.07

^a Only transitions with oscillator strength higher than 0.01 are shown. ^b Numbers between parenthesis represent transition coefficients.

only accounts for the reduction of the band gap and bathochromic shift of the visible absorptions but also represents an opposite trend (also observed with *Pc* fused dimers¹⁹) as that observed for the frontier orbitals of mononuclear π -conjugated macrocycles (naphthalocyanines, anthracocyanines, etc.^{18,20}). In the later chromophores, both HOMO and LUMO orbitals become less stable with increasing extension of π -conjugation, in particular the HOMO is strongly destabilized (thus the net effect is a band gap decrease). This overall destabilization of the frontier orbitals could be a possible explanation for the lower stability of mononuclear π -extended structures, with respect to polynuclear analogues that absorb at similar wavelengths (for example, subnaphthalocyanines *vs* Dimers).

The peripheral substitution alters significantly the orbital energies in that acceptor substituents such as fluorine atoms stabilize the orbitals systematically, while weaker acceptor substituents such as iodine atoms produce a smaller stabilization (Figure 12).

Thioether donor groups (**7a**) have an overall minimum destabilization effect on the frontier orbital, with respect to the unsubstituted SubPc Dimers **8a,b**, although in this compound the HOMO-2 orbital, that corresponds to the *n* orbital of the sulfur atoms, is strongly destabilized, being close to the HOMO-1. This destabilization accounts for the appearance of $n \rightarrow \pi^*$ transitions around 400 nm in the UV spectra. Axial substitution has no significant effects in the orbital shape and energies, as most frontier orbitals have no contributions in the axial substituents or in the boron atom. This is in agreement with the observed negligible changes in the UV spectra upon axial functionalization.

As a result of the frontier orbital split-up, the UV–vis absorption spectra of the SubPcDimers present a very distinct Q band in which four peaks are clearly defined, where the one in the red end being the most intense, followed by the one on the blue end (Figure 7).

In an effort to assign the orbital transitions to the observed UV–vis peaks in the Q band, a time-dependent DFT (TDDFT) calculation of the electronic excitations was performed on the SubPcDimers **1a**. As solvation effects are not taken into account in this calculation, the transitions are systematically shifted to the blue with respect to the experimental spectra.²¹ The calculation results show 5 transitions for the Q band, ranging

from the HOMO-1 → LUMO+3 to the HOMO → LUMO (Table 6).

Concluding Remarks

New SubPc-fused Dimers and Trimers bearing donor and acceptor substituents in their peripheral positions were synthesized and characterized. Photophysical and electrochemical studies revealed (i) that the substituents have a strong effect on the electronic properties of the macrocycles and (ii) that there is good communication between the subphthalocyaninic moieties within the oligomeric structures. Theoretical calculations at DFT/6-31G(d,p) computational level along with electron density studies support the experimental findings. The frontier orbitals in the Dimers and Trimers were shown to be significantly altered with respect to those of SubPcs as a consequence of the extension of the conjugation associated with symmetry breaking. TDDFT calculations were shown to reproduce the differences observed in the UV–vis spectra of the Dimers and the SubPcs.

Experimental Section

Computational Method. DFT and AM1 calculations were performed using the Gaussian03²² program package. Strict C_{3v} , C_{2v} , and C_1 symmetry conditions were imposed for geometry optimizations of the SubPc monomers, the Dimer *syn*, and the Dimer *anti*, respectively. The functional used in DFT calculations was the B3LYP,²³ and the basis sets selected were the 6-31G(d,p). Semiempirical AM1 calculations were performed for estimating the heat of formation of the studied compounds as well as for the geometry optimization of some molecules having atoms not defined for the 6-31G(d,p) basis sets. The electronic transitions for compound **8a** were calculated, over the DFT optimized structures, using the time-dependent DFT (TDDFT) methodology at 6-31G(d,p) level with the same B3LYP functional, spanning 8 orbitals (4 virtual and 4 occupied). Single and double cations and anions were calculated

(19) Kobayashi, N.; Lam, H.; Nevin, W. A.; Janda, P.; Leznoff, C. C.; Koyama, T.; Monden, A.; Shirai, H. *J. Am. Chem. Soc.* **1994**, *116*, 879–890.

(20) Kobayashi, N.; Nakajima, S.; Ogata, H.; Fukuda, T. *Chem.–Eur. J.* **2004**, *10*, 6294–6312.

(21) (a) Mennucci, B.; Toniolo, A.; Tomasi, J. *J. Phys. Chem. A* **2001**, *105*, 4749–4757. (b) Jacquemin, D.; Preat, J.; Wathelet, V.; Fontaine, M.; Perpète, E. A. *J. Am. Chem. Soc.* **2006**, *128*, 2072–2083.

(22) Frisch, M. J.; Trucks, G. W.; Schlegel, H. B.; Scuseria, G. E.; Robb, M. A.; Cheeseman, J. R.; Montgomery, J. A., Jr.; Vreven, T.; Kudin, K. N.; Burant, J. C.; Millam, J. M.; Iyengar, S. S.; Tomasi, J.; Barone, V.; Mennucci, B.; Cossi, M.; Scalmani, G.; Rega, N.; Petersson, G. A.; Nakatsuji, H.; Hada, M.; Ehara, M.; Toyota, K.; Fukuda, R.; Hasegawa, J.; Ishida, M.; Nakajima, T.; Honda, Y.; Kitao, O.; Nakai, H.; Klene, M.; Li, X.; Knox, J. E.; Hratchian, H. P.; Cross, J. B.; Bakken, V.; Adamo, C.; Jaramillo, J.; Gomperts, R.; Stratmann, R. E.; Yazyev, O.; Austin, A. J.; Cammi, R.; Pomelli, C.; Ochterski, J. W.; Ayala, P. Y.; Morokuma, K.; Voth, G. A.; Salvador, P.; Dannenberg, J. J.; Zakrzewski, V. G.; Dapprich, S.; Daniels, A. D.; Strain, M. C.; Farkas, O.; Malick, D. K.; Rabuck, A. D.; Raghavachari, K.; Foresman, J. B.; Ortiz, J. V.; Cui, Q.; Baboul, A. G.; Clifford, S.; Cioslowski, J.; Stefanov, B. B.; Liu, G.; Liashenko, A.; Piskorz, P.; Komaromi, I.; Martin, R. L.; Fox, D. J.; Keith, T.; Al-Laham, M. A.; Peng, C. Y.; Nanayakkara, A.; Challacombe, M.; Gill, P. M. W.; Johnson, B.; Chen, W.; Wong, M. W.; Gonzalez, C.; Pople, J. A. *Gaussian 03*, Revision C.02; Gaussian, Inc.: Wallingford CT, 2004.

(23) Becke, A. D. *J. Chem. Phys.* **1993**, *98*, 5648–5652.

at 6-31+G(d,p) computational level. The electron density analysis was carried out by the method of deformed atoms in molecules (DAM).²⁴ In this method, the molecular electron density is partitioned into minimally deformed pseudoatomic densities, which are achieved by assigning to each atom the charge distributions centered on its nucleus plus the parts of the two-center ones nearest to it. The resulting *atoms* (actually, pseudoatomic fragments) keep an almost spherical shape with slight deformations caused by the molecular environment, thus connecting with the intuitive view of atoms in molecules shared by the great majority of the chemical community. Furthermore, the small deformations of every atom can be separated from the largely dominant spherical term, and are easily decomposed in multipole-type components (dipole, quadrupole, octapole, etc.), the corresponding effective multipoles being represented by analytical functions of the distance in a straightforward manner. As it has been recently proved,²⁴ the analysis of these deformations brings much insight about the lone pairs of atoms and bond scheme in molecules. The DAM calculations were performed by the program package developed by Fernández Rico and co-workers.²⁴ The electron density plots were visualized with the gOpenMol program.²⁵ Contour surfaces of the electron density deformations were obtained for different contour values but taking especially into account those corresponding to 0.001 au because it has been solidly proved that typical aromatic compounds like benzene exhibit a characteristic delocalization pattern at this deformation level.

Compounds 1a–f. BCl₃ (10.1 mL of a 1 M solution in *p*-xylene) was added dropwise to a solid mixture of tetrafluorophthalonitrile (561 mg, 2.81 mmol) and 1,2,4,5-benzenetetracarboxitrile (50 mg, 0.28 mmol) under argon and magnetic stirring. The reaction mixture was refluxed for 3 h and after cooling down to room temperature was flushed with argon. The resulting dark-purple slurry was then evaporated under vacuo. SubPc (**1f**) was separated from Dimers and Trimers (compounds **1a–e**) by column chromatography on silica gel using dichloromethane/hexane (3:2) as eluent. Dimers **1a** and **1b** and Trimers **1c–e** were further separated using hexane/acetone (1:4) as eluent.

Dimer 1a. Blue-reddish powder, 33 mg (11%); mp > 250 °C; ¹H NMR (300 MHz, CDCl₃, 25 °C): δ = 10.46 ppm (s); IR (KBr): ν̄ = 1535, 1481, 1400, 1273, 1219, 1165, 1111, 1070, 1016, 966, 856, 795, 708, 658, 586 cm⁻¹; UV/vis (CHCl₃): λ_{max}(log(ε)) = 692 (4.9), 662 (4.4), 636 (4.4), 605 (4.5), 592 (sh), 441 (3.9), 320 (4.5), 278 nm (4.4); MALDI-TOF: *m/z* 1071.7 [M⁺] and [M⁺+H]; HR-LSIMS calcd for C₄₂H₂N₁₂F₁₆B₂Cl₂ [M⁺] *m/z* 1069.9833, found 1069.9825; elemental analysis calcd (%) for C₄₂H₂N₁₂F₁₆B₂Cl₂: C 47.10, H 0.19, N 15.69; found: C 47.61, H 0.31, N 15.51.

Dimer 1b. Blue-reddish powder, 27 mg (9%); mp > 250 °C; ¹H NMR (300 MHz, CDCl₃, 25 °C): δ = 10.48 ppm (s); IR (KBr): ν̄ = 1539, 1487, 1400, 1285, 1225, 1165, 1067, 1020, 962, 858, 789, 638, 592, 557 cm⁻¹; UV/vis (CHCl₃): λ_{max}(log(ε)) = 693 (4.9), 661 (4.4), 635 (4.4), 604 (4.5), 592 (sh), 441 (3.7), 319 (4.5), 278 nm (4.4); MALDI-TOF: *m/z* 1070.7 [M⁺] and [M⁺+H]; HR-LSIMS calcd for C₄₂H₂N₁₂F₁₆B₂Cl₂ [M⁺] *m/z* 1069.9833, found 1069.9845; elemental analysis calcd (%) for C₄₂H₂N₁₂F₁₆B₂Cl₂: C 47.10, H 0.19, N 15.69; found: C 47.56, H 0.26, N 15.25.

Trimers 1c–e. Dark-blue powder, 6 mg (3%); mp > 250 °C; ¹H NMR (300 MHz, CDCl₃, 25 °C): δ = 10.58 (s), 10.53 (s), 10.51 (s), 10.48 (s), 10.44 ppm (s); IR (KBr): ν̄ = 1733, 1625,

1537, 1517, 1483, 1402, 1281, 1220, 1166, 1112, 1058, 1017, 858, 794, 706, 653, 578 cm⁻¹; UV/vis (CHCl₃): λ_{max}(log(ε)) = 755 (4.9), 697 (4.6), 661 (4.5), 637 (4.4), 585 (4.5), 317 (4.6), 280 nm (4.6); MALDI-TOF: *m/z* 1495.6 [M⁺]; HR-LSIMS calcd for C₆₀H₄N₁₈F₂₀B₃Cl₃ [M⁺] *m/z* 1493.9892, found 1493.9936; elemental analysis calcd (%) for C₆₀H₄N₁₈F₂₀B₃Cl₃: C 48.19, H 0.27, N 16.86; found: C 48.54, H 0.41, N 16.33.

SubPc 1f. Purple powder, 260 mg (43%). Compound possessing identical physical properties as described previously.¹⁰

Compounds 2a,b,f: Method A. A mixture of phenol (500 mg, 5.3 mmol) and the crude product from the previous reaction in toluene (2 mL) was warmed up to reflux overnight. The resulting solid was then subjected to various column chromatographies on silica gel using dichloromethane, ethyl acetate/hexane (1/4), and acetone/hexane (1:0 to 1:4) as successive eluents.

Dimer 2a. Dark-blue powder, 23 mg (7%); mp > 250 °C; ¹H NMR (300 MHz, CDCl₃, 25 °C): δ = 10.36 (s, 2H), 6.905–6.72 (m, 6H), 5.49 ppm (d, *J* = 8.2 Hz, 4H); IR (KBr): ν̄ = 1531, 1477, 1396, 1265, 1225, 1103, 995, 903, 760, 708, 644, 594 cm⁻¹; UV/vis (CHCl₃): λ_{max}(log(ε)) = 689 (4.9), 657 (4.4), 631 (4.4), 601 (4.5), 586 (sh), 441 (3.9), 319 (4.5), 273 nm (4.5); MALDI-TOF: *m/z* 1186.8 [M⁺] and [M⁺+H]; HR-LSIMS calcd for C₅₄H₁₂N₁₂F₁₆B₂O₂ [M⁺] *m/z* 1187.1137, found 1187.1190; elemental analysis calcd (%) for C₅₄H₁₂N₁₂F₁₆B₂O₂: C 54.67, H 1.02, N 14.17; found: C 54.95, H 1.27, N 13.64.

Dimer 2b. Dark-blue powder, 20 mg (6%); mp > 250 °C; ¹H NMR (300 MHz, CDCl₃, 25 °C): δ = 10.40 (s, 2H), 6.75–6.60 (m, 6H), 5.36 ppm (d, *J* = 7.6 Hz, 4H); IR (KBr): ν̄ = 1529, 1477, 1393, 1275, 1213, 1161, 1107, 1080, 968, 899, 702, 644, 598 cm⁻¹; UV/vis (CHCl₃): λ_{max}(log(ε)) = 688 (4.9), 657 (4.4), 631 (4.4), 600 (4.5), 587 (sh), 441 (3.7), 319 (4.4), 274 nm (4.3); MALDI-TOF: *m/z* 1186.9 [M⁺] and [M⁺+H]; HR-LSIMS calcd for C₅₄H₁₂N₁₂F₁₆B₂O₂ [M⁺] *m/z* 1187.1137, found 1187.1146; elemental analysis calcd (%) for C₅₄H₁₂N₁₂F₁₆B₂O₂: C 54.67, H 1.02, N 14.17; found: C 55.11, H 1.32, N 13.77.

SubPc 2f. Purple powder, 224 mg (34%). Compound possessing identical physical properties as described previously.¹⁰

Method B. A 1:1 mixture of Dimers **1a–b** (48 mg, 0.044 mmol) was reacted with phenol (42 mg, 0.44 mmol, 10 eq.) in toluene (1 mL) at reflux overnight. The workup was identical as the one described in Method A. Dimer **2a**, 16 mg. Dimer **2b**, 18 mg (66%).

Compounds 3a,b,f: Method A. 0.970 g (5.6 mmol) of tetrafluorophthalonitrile, 0.1 g (0.56 mmol) of 1,2,4,5-tetracyanobenzene, and 6.2 mL (6.2 mmol) of BCl₃ solution in *p*-xylene. Reaction time: 2 h.

1.54 g (10.2 mmol) of 4-*tert*-butylphenol. Phenol reaction time: 30 h (solvent: toluene (1 mL)). Crude washed with MeOH/H₂O 5:1.

A first column in silica gel using hexane/dichloromethane (1:1) as eluent separated the corresponding SubPc **3f** from the Dimers **3a** and **3b**. The second column chromatography (hexane/acetone 3:1) separated **3a** from **3b**.

Dimer 3a. Dark-blue solid, 58 mg (8%); mp > 250 °C; ¹H NMR (300 MHz, CDCl₃): δ = 10.37 (s, 2H), 6.87 (d, *J*_o = 8.8 Hz, 4H), 5.41 (d, *J*_o = 8.8 Hz, 4H), 1.15 ppm (s, 18H); IR (KBr): ν̄ = 2961, 2360, 1625, 1533, 1483, 1393, 1260, 1217, 1099, 996, 963, 902 cm⁻¹; UV-vis (CHCl₃): λ_{max}(log(ε)) = 689 (4.9), 657 (4.5), 633 (4.5), 601 (4.6), 589 (sh), 449 (3.9), 317 nm (4.6); MALDI-TOF: *m/z* 1299 [M]⁺, 1149 [M-one axial group]⁺; elemental analysis calcd for C₆₂H₂₈B₂F₁₆N₁₂O₂: C, 57.35; H, 2.17; N, 12.94; found: C, 57.19; H, 1.99; N, 12.79.

Dimer 3b. Dark-blue solid, 80 mg (11%); mp > 250 °C; ¹H NMR (300 MHz, CDCl₃): δ = 10.40 (s, 2H), 6.72 (d, *J*_o = 8.8 Hz, 4H), 5.26 (d, *J*_o = 8.8 Hz, 4H), 1.02 ppm (s, 18H); IR (KBr): ν̄ = 2962, 1633, 1533, 1482, 1393, 1364, 1265, 1217, 1107, 998, 963, 902, 830 cm⁻¹; UV-vis (CHCl₃): λ_{max}(log(ε)) = 688 (4.8), 656 (4.3), 631 (4.4), 600 (4.4), 588 (sh), 439 (3.8), 314 nm (4.5); MALDI-TOF: *m/z* 1299 [M + H]⁺, 1149 [M + H-one axial

(24) (a) Fernández Rico, J.; López, R.; Ema, I.; Ramírez, G. J. *Chem. Theory Comput.* **2005**, *1*, 1083–1095. (b) Fernández Rico, J.; López, R.; Ramírez, G. J. *Chem. Phys.* **1999**, *110*, 4213–4220. (c) Fernández Rico, J.; López, R.; Ema, I.; Ramírez, G. J. *Comput. Chem.* **2004**, *25*, 1347–1354. (d) Fernández Rico, J.; López, R.; Ramírez, G.; Ema, I.; Ludeña, E. V. J. *Comput. Chem.* **2004**, *25*, 1355–1363.

(25) (a) Laaksonen, L. J. *Mol. Graphics* **1992**, *10*, 33–34. (b) Bergman, D. L.; Laaksonen, L.; Laaksonen, A. J. *Mol. Graphics* **1997**, *15*, 300–306. (c) gOpenMol is a freeware program that can be found in: www.csc.fi/gopenmol/.

group]⁺; elemental analysis calcd for C₆₂H₂₈B₂F₁₆N₁₂O₂: C, 57.35; H, 2.17; N, 12.94; found: C, 57.22; H, 2.25; N, 12.83.

SubPc 3f. Purple powder, 550 mg (45%); mp > 250 °C; ¹H NMR (300 MHz, CDCl₃): 6.80 (d, *J*_o = 8.9 Hz, 2H), 5.27 (d, *J*_o = 8.9 Hz, 2H), 1.10 (s, 9H); IR (KBr): $\bar{\nu}$ = 2963, 1632, 1535, 1484, 1221, 1165, 1112, 966 cm⁻¹; UV-vis (CHCl₃): λ_{max} (log(ϵ)): 570 (4.7), 555 (sh), 530 (4.2), 307 nm (4.4); MALDI-TOF: *m/z* = 761 [M + H]⁺; elemental analysis calcd for C₃₄H₁₃-BF₁₂N₆O: C, 53.71; H, 1.72; N, 11.05; found: C, 53.88; H, 1.69; N, 10.98.

Method B. A 1:1 mixture of Dimers **1a–b** (52 mg, 0.049 mmol) was reacted with 4-*tert*-butylphenol (46 mg, 0.49 mmol, 10 equiv) in toluene (1 mL) at reflux overnight. The workup was identical as the one described in Method A. Dimer **3a**, 22 mg. Dimer **3b**, 26 mg (75%).

Compounds **5a,b,f**: BCl₃ (6.2 mL of a 1 M solution in *p*-xylene) was added dropwise to a solid mixture of 4-iodophthalonitrile (1.4 g, 5.6 mmol) and 1,2,4,5-benzenetetracarboxynitrile (0.1 g, 0.56 mmol) under argon and magnetic stirring. The reaction mixture was refluxed for 2 h and after cooling down to room temperature was flushed with argon. The resulting dark-purple slurry was then evaporated under vacuo. 1.54 g (10.2 mmol) of 4-*tert*-butylphenol and toluene (1 mL) were then added, and the resulting solution was refluxed for 30 h. The resulting reaction crude was washed with MeOH/H₂O 5:1. The first column chromatography on silica gel using toluene as eluent separated the corresponding SubPc **5f** from the Dimers **5a** and **5b**. Further column chromatographies using toluene/dichloromethane (1:1), hexane/acetone (3:1), and dichloromethane/hexane (3:1) isolated three groups of Dimers **5a**, **5b**, and **5b'**.

Compound 5a. Dark-blue solid, 6 mg (0.7%); mp > 250 °C; ¹H NMR (300 MHz, CDCl₃): δ = 10.21 (s, 2H), 9.22–9.13 (m, 4H), 8.57–8.39 (m, 4H), 8.20–8.07 (m, 4H), 6.90–6.83 (m, 4H), 5.48–5.41 (m, 4H), 1.14 ppm (s, 18H); IR (KBr): $\bar{\nu}$ = 2924, 1853, 1636, 1508, 1458, 1384, 1260, 1180, 1124, 1068. cm⁻¹; UV-vis (CHCl₃): λ_{max} (log(ϵ)): 706 (4.8), 675 (4.3), 647 (4.3), 609 (4.4), 599 (sh), 441 (3.8), 339 nm (4.4); MALDI-TOF: *m/z* 1515 [M + H]⁺, 1365 [M + H-one axial group]⁺; HR-LSIMS calcd for C₆₆H₅₆B₂L₄N₁₂O₂: [M]⁺; *m/z*: 1578.1014, found 1578.0953.

Compounds 5b' and 5b". 5b'. Dark-blue solid, 9 mg (1%); mp > 250 °C; ¹H NMR (300 MHz, CDCl₃): δ = 10.30 (s, 2H), 9.33–9.25 (m, 4H), 8.70–8.58 (m, 4H), 8.31–8.26 (m, 4H), 6.68 (d, *J*_o = 8.8 Hz, 4H), 5.25 (d, *J*_o = 8.8 Hz, 4H), 1.00 ppm (s, 18H); IR (KBr): $\bar{\nu}$ = 2923, 1636, 1458, 1261, 1124, 1090, 1059 cm⁻¹; UV-vis (CHCl₃): λ_{max} (log(ϵ)): 700 (4.9), 672 (4.6), 644 (4.5), 606 (4.6), 443 (4.0), 336 nm (4.6); MALDI-TOF: *m/z* 1515 [M + H]⁺, 1365 [M + H-one axial group]⁺; HR-LSIMS calcd for C₆₆H₅₆B₂L₄N₁₂O₂: [M]⁺; *m/z* 1578.1014, found 1578.1067.

5b". Dark-blue solid, 4 mg (0.5%); mp > 250 °C; ¹H NMR (300 MHz, CDCl₃): δ = 10.30 (s, 2H), 9.33–9.25 (m, 4H), 8.71–8.58 (m, 4H), 8.31–8.26 (m, 4H), 6.69 (d, *J*_o = 8.8 Hz, 4H), 5.26 (d, *J*_o = 8.8 Hz, 4H), 1.00 ppm (s, 18H); IR (KBr): $\bar{\nu}$ = 2960, 2924, 2854, 1602, 1507, 1458, 1377, 1261, 1094, 1041 cm⁻¹; UV-vis (CHCl₃): λ_{max} (log(ϵ)): 704 (4.9), 672 (4.6), 643 (4.5), 607 (4.6), 443 (4.0), 321 nm (4.6); MALDI-TOF: *m/z* 1515 [M + H]⁺, 1365 [M + H-one axial group]⁺; HR-LSIMS calcd for C₆₆H₅₆B₂L₄N₁₂O₂: [M]⁺; *m/z* 1578.1014, found 1578.0989.

Compound **5f** was isolated by column chromatography in silica gel (toluene as eluent) as two regioisomers: C₃ (**5f'**) and C₁ (**5f''**).

5f' (C₃). Purple powder, 150 mg (9%); mp > 250 °C; ¹H NMR (300 MHz, CDCl₃): δ = 9.19 (s, 3H), 8.54 (d, *J*_o = 8.5 Hz), 8.20 (dd, *J*_o = 8.5 Hz, *J*_m = 1.2 Hz, 3H), 6.75 (d, *J*_o = 8.5 Hz, 2H), 5.26 (d, *J*_o = 8.5 Hz, 2H), 1.08 (s, 9H); IR (KBr): $\bar{\nu}$ = 2923, 1602, 1509, 1460, 1438, 1303, 1259, 1177, 1057 cm⁻¹; UV-vis (CHCl₃): λ_{max} (log(ϵ)): 571 (4.5), 530 (sh), 318 nm (4.1); MALDI-TOF: *m/z* 923 [M + H]⁺, 773 [M + H-axial group]⁺; elemental analysis calcd for C₃₄H₂₂BI₃N₆O: C, 44.29; H, 2.40; N, 9.11; found: C, 44.05; H, 2.56; N, 9.30.

5f'' (C₁). Purple powder, 450 mg (27%); mp > 250 °C; ¹H NMR (300 MHz, CDCl₃): δ = 9.16–9.19 (m, 3H), 8.52–8.56 (m, 3H), 8.18–8.22 (m, 3H), 6.75 (d, *J*_o = 8.6 Hz, 2H), 5.26 (d, *J*_o = 8.6 Hz, 2H), 1.08 (s, 9H); IR (KBr): $\bar{\nu}$ = 2957, 1601, 1511, 1460, 1442, 1310, 1290, 1257, 1177, 1062, 1039 cm⁻¹; UV-vis (CHCl₃): λ_{max} (log(ϵ)): 571 (4.8), 530 (sh), 320 nm (4.4); MALDI-TOF: *m/z* 923 [M + H]⁺, 773 [M + H-axial group]⁺; elemental analysis calcd for C₃₄H₂₂BI₃N₆O: C, 44.29; H, 2.40; N, 9.11; found: C, 44.02; H, 2.51; N, 9.23.

Compounds 7a,b,f. BCl₃ (1.85 mL of a 1 M solution in *p*-xylene) was added dropwise to a solid mixture of 4,5-diethylthiophthalonitrile (700 mg, 1.7 mmol) and 1,2,4,5-benzenetetracarboxynitrile (30 mg, 0.17 mmol) under argon and magnetic stirring. The reaction mixture was refluxed for 3 h and after cooling down to room temperature, was flushed with argon. The resulting dark-purple slurry was then evaporated under vacuo. 460 mg (3 mmol) of 4-*tert*-butylphenol and toluene (1.5 mL) were then added, and the resulting solution was refluxed for 18 h. The resulting reaction crude was washed with MeOH/H₂O 5:1. Column chromatography on silica gel (hexane/acetone 30:1) separated the correspondent SubPc **7f** from the Dimers **7a–b**. A second column in hexane/dichloromethane 1:1 separated the two topoisomers.

Compound 7a. Viscous green solid, 33 mg (9%); mp > 250 °C; ¹H NMR (300 MHz, CDCl₃): 10.29 (s, 2H), 8.66 (s, 4H), 8.55 (s, 4H), 6.84 (d, *J*_o = 8.6 Hz, 4H), 5.44 (d, *J*_o = 8.6 Hz, 4H), 3.32–3.17 (m, 16H), 1.95–1.80 (m, 16H), 1.70–1.47 (m, 16H), 1.45–1.10 (m, 64H), 1.13 (s, 18H), 0.95–0.78 (m, 24H); IR (KBr): $\bar{\nu}$ = 2925, 2853, 1597, 1458, 1259, 1126, 1061 cm⁻¹; UV-vis (CHCl₃): λ_{max} (log(ϵ)): 739 (5.0), 704 (4.6), 676 (4.5), 630 (sh), 605 (4.7), 421 (4.7), 294 nm (5.1); MALDI-TOF: *m/z* 2164 [M + H]⁺, 2015 [M + H-one axial group]⁺; elemental analysis calcd for C₁₂₆H₁₇₂B₂N₁₂O₂S₈: C, 69.90; H, 8.01; N, 7.76; found: C, 69.90; H, 8.20; N, 7.68.

Compound 7b. Viscous green solid, 26 mg (7%); mp > 250 °C; ¹H NMR (300 MHz, CDCl₃): 10.29 (s, 2H), 8.69 (s, 4H), 8.63 (s, 4H), 6.69 (d, *J*_o = 8.8 Hz, 4H), 5.31 (d, *J*_o = 8.8 Hz, 4H), 3.43–3.20 (m, 16H), 1.97–1.84 (m, 16H), 1.72–1.50 (m, 16H), 1.51–1.16 (m, 64H), 1.01 (s, 18H), 0.96–0.80 (m, 24H); IR (KBr): $\bar{\nu}$ = 2925, 2854, 1603, 1461, 1260, 1125, 1079 cm⁻¹; UV-vis (CHCl₃): λ_{max} (log(ϵ)): 736 (5.0), 703 (4.6), 672 (4.5), 629 (4.6), 620 (sh), 430 (4.4), 336 (sh), 298 nm (4.8); MALDI-TOF: *m/z* 2164 [M + H]⁺, 2015 [M + H-one axial group]⁺; elemental analysis calcd for C₁₂₆H₁₇₂B₂N₁₂O₂S₈: C, 69.90; H, 8.01; N, 7.76; found: C, 69.77; H, 8.18; N, 7.67.

Compound 7c–e. Light-green solid, 1 mg (0.2%); mp > 250 °C; ¹H NMR (300 MHz, CDCl₃): 10.39 (s, 2H), 10.34 (s, 2H), 8.78–8.57 (m, 10H), 6.88–6.63 (m, 6H), 5.49–5.33 (m, 6H), 3.30–3.20 (m, 20H), 1.95–1.80 (m, 20H), 1.70–1.50 (m, 20H), 1.45–1.20 (m, 80H), 1.15–1.00 (m, 27H), 0.95–0.8 (m, 30H); IR (KBr): $\bar{\nu}$ = 2924, 2854, 1461, 1261, 1082, 1025, 803, 698 cm⁻¹; UV-vis (CHCl₃): λ_{max} (log(ϵ)): 807 (5.0), 735 (4.9), 697 (4.8), 617 (4.7), 433 (4.6), 350 (sh), 298 nm (5.0); HR-LSIMS calcd for C₁₇₀H₂₂₅B¹¹B₂N₁₈O₃S₁₀: [M]⁺; *m/z* 2916.537327, found 2916.547100.

Compound 7f. Red-blue viscous solid (310 mg, 39%); mp > 250 °C; ¹H NMR (300 MHz, CDCl₃): 8.59 (s, 6H), 6.77 (d, *J*_o = 8.9 Hz, 2H), 5.33 (d, *J*_o = 8.9 Hz, 2H), 3.33–3.17 (m, 12H), 1.91–1.81 (m, 12H), 1.65–1.54 (m, 12H), 1.45–1.28 (m, 48H), 1.09 (s, 9H), 0.92–0.85 (m, 18H); IR (KBr): $\bar{\nu}$ = 2924, 2853, 1597, 1511, 1459, 1418, 1258, 1181, 1079, 1055, 816 cm⁻¹; UV-vis (CHCl₃): λ_{max} (log(ϵ)): 599 (5.0), 560 (sh), 406 (4.5), 389 (4.5), 298 (4.8) nm; MALDI-TOF: *m/z* 1409 [M + H]⁺, 1260 [M + H-axial group]⁺; elemental analysis calcd for C₈₂H₁₂₁BN₆OS₆: C, 69.85; H, 8.65; N, 5.96; found: C, 69.66; H, 8.86; N, 5.98.

Compound 9. Mp > 250 °C; ¹H NMR (300 MHz, CDCl₃): 9.39 (s, 2H), 8.22 (s, 1H); IR (KBr): $\bar{\nu}$ = 2926, 1776, 1730, 1514, 1406, 1282, 1120, 1040 cm⁻¹; UV-vis (CHCl₃): λ_{max} (log(ϵ)): 586 (4.7), 573 (4.6), 545 (4.3), 523 (4.2), 310 (4.5), 280 (sh), 241 (4.6) nm; HR-LSIMS calcd for C₂₆H₃BCIF₈N₇O₂: [M]⁺; *m/z*: 643.00021, found 643.00214.

Compound 11. Mp > 250 °C; ^1H NMR (300 MHz, CDCl_3): 7.90 (s, 1H); IR (KBr): $\bar{\nu}$ = 3230, 3092, 2731, 1788, 1721, 1643, 1499, 1406, 1300, 1141, 1038, 920, 756, 652; HR-EI calcd for $\text{C}_8\text{HNO}_2\text{F}_4$: $[\text{M}^+]$: 218.9943, found 218.9940.

Acknowledgment. This work was supported by the Spanish MEC (CTQ-2005-08933-BQU, MAT2004-03849, “Ramón y Cajal” Program) and the Comunidad de Madrid (S-0505/PPQ/000225). RSI would like to thank the Coordenação de Aperfeiçoamento de Pessoal de Nível Superior (CAPES, Brazil) for the grant conceded to accomplish this work. The electrochemical measurements were performed in the laboratory of Prof. Nazario

Martín at Complutense University of Madrid to whom we are very grateful. MAH would also like to thank Profs. Martín and Echegoyen for their continuous support.

Supporting Information Available: Instrumentation, Spectroscopic data for compounds **3a**, **3b**, **3f**, **5a**, **5b'**, **5f'**, **5f''**, **7a**, **7b**, **7c–e**, **7f**, **9**, and **11** (^1H NMR, UV–vis, IR, and MS) and optimized molecular modeling coordinates for compound **1a,b,e,f** and **8a,b,e,f**. This material is available free of charge via the Internet at <http://pubs.acs.org>.

JO062608H